

Revisiting the Exposed Surface Characteristics on the Stability and Photoelectric Properties of MAPbI₃

Bingdong Zhang,^[a, b] Ruiyang Shi,^[a] Hongke Ma,^[c] Kai Ma,^[a, b] Zhengyang Gao,^[a, b] and Hao Li^{*[d]}

CH₃NH₃PbI₃ (MAPbI₃), as a promising candidate of photovoltaic materials, has attracted extensive interests due to its excellent photoelectric properties and low preparation cost. However, the relationship between synthesis parameter and performance is still unclear due to the overlook of exposed surface characteristics, limiting the mass-production and commercialization of MAPbI₃. Therefore, it is necessary to clarify the stability and photoelectric properties of different exposed surfaces of MAPbI₃ under humid environment. In this work, the stability and photoelectric properties of the MAI-terminated and PbI₂-terminated of MAPbI₃ (001) were thoroughly investigated using density functional theory calculation. To study the stability of exposed surface, adsorption energy of water molecules, ab initio molecular dynamics (AIMD), mean square displacement (MSD) and X-ray diffraction (XRD) were calculated. MSD of PbI₂-terminated surface is greater by two orders of magnitude

compared to MAI-terminated surface. For the photoelectric properties of MAPbI₃, the bandgap, absorption coefficients, joint density of states (JDOS) and dielectric constants were investigated. The inhibitory effect of water on the photoelectric performance for PbI₂-terminated surface is more significant than that of MAI-terminated surface. Although the photoelectric properties of water molecules adsorption on MAI-terminated surface is basically unchanged, the diffusion of water molecules reduces the photoelectric properties of MAPbI₃. Overall, the stability and photoelectric properties of MAI-terminated surface are superior to PbI₂-terminated surface. Therefore, we strongly advocate paying attention to the exposed surface of MAPbI₃ during the thin film production process and adjusting synthesis parameters to prepare MAI-terminated surface dominated thin film, which should substantially improve the performance of MAPbI₃ in the application.

1. Introduction

After CH₃NH₃PbI₃ (MAPbI₃) was first employed in photovoltaic solar cells, achieving an efficiency of 3.8%,^[1] it was considered a promising material due to its long electron and hole diffusion lengths, tunable optical bandgap, high carrier mobility, high light absorption coefficient, and low production cost.^[2] In contrast to the slow development of silicon cells, the efficiency of perovskite solar cell has gone to 25.7% in the last decade,^[3] which is comparable to single-crystal silicon materials.^[4] Although the rapid development of MAPbI₃ in the last decade, a desirable MAPbI₃ for photovoltaics with high photoelectric efficiency and stable operation for 25 years which obviously hinders its practical application.^[5]

Water in a humid environment is important for the stable operation of MAPbI₃,^[6] but its effect on the photoelectric efficiency is still disputed. For the stable operation, MAPbI₃ reacts easily with water in a humid environment, which can seriously damage its stability.^[7] Zhao et al.^[8] found that when water is added to MAPbI₃ powder, it will immediately decompose to produce PbI₂. Therefore, its preparation should in a glovebox filled with inert gas to prevent the adverse effects of water.^[9] However, many research proved that the presence of water molecules may improve the photoelectric properties of MAPbI₃. You et al.^[10] found that their annealing fabrication efficiency in ambient air was higher than that in nitrogen and pure oxygen, proving that the presence of water increases the efficiency of MAPbI₃. Kim et al.^[11] found that at specific humidity levels, without any additives, the density of bulk defects and interface composite sites were significantly reduced, resulting in the formation of larger grains and improved optical quality. Zhu et al.^[12] found that exposure to humid environments can increase grain size, which reduces defect states and grain boundaries. Although the morphology of MAPbI₃ synthesized in high humidity environment is not perfect, it possesses higher open circuit voltage, photoluminescence and quantum yield.^[13] More importantly, Dong et al.^[14] found that the photocatalytic performance of MAI-terminated surface is superior to PbI₂-terminated surface, which facilitates the carrier transport. Therefore, the properties of various exposed surfaces are also critical for the photoelectric effect.

Recently, several studies have shown the stability of different exposed surfaces in humid environment. Mosconi et al.^[15]

[a] B. Zhang, R. Shi, K. Ma, Z. Gao
Department of Power Engineering, North China Electric Power University, Baoding, Hebei 071003, China

[b] B. Zhang, K. Ma, Z. Gao
Hebei Key Laboratory of Low Carbon and High-Efficiency Power Generation Technology, North China Electric Power University, Baoding, Hebei 071003, China

[c] H. Ma
FTXT Energy Technology Co., Ltd., Baoding 071000, China

[d] H. Li
Advanced Institute for Materials Research (WPI-AIMR), Tohoku University, Sendai 980-8577, Japan
E-mail: li.hao.b8@tohoku.ac.jp

Supporting information for this article is available on the WWW under <https://doi.org/10.1002/cphc.202400897>

found that the MAI-terminated surface underwent rapid solvation with a water molecule replacing the iodine atom on the MAI-terminated surface, while the PbI_2 -terminated surface did not undergo a similar phenomenon. Lu et al.^[16] found that although both surfaces of the film produced PbI_2 in a humid environment, the PbI_2 -terminated surface was less stable than the MAI-terminated surface. Nachimuthu et al.^[17] found that in MAPbI_3 material, significant structural degradation occurs on the surface when PbI_2 is exposed to light, H_2O , and O_2 simultaneously, while the MAI exposed surface remains stable. Ouyang et al.^[18] revealed that moisture can promote the oxidation of those two exposed surfaces, especially the PbI_2 -terminated surface. However, little has been explored about the changes in the photoelectric properties of the two explore surfaces in a humid environment, which also has important implications for the use of MAPbI_3 .

Motivated by the aforementioned landscape, this work investigates the stability and photoelectric properties of two exposed surfaces of MAPbI_3 using density functional theory calculations. First, the Gibbs adsorption energy of water molecules adsorbed on both surfaces was calculated. Second, The MAI-terminated was found to be more stable than the PbI_2 -terminated by analysis. Third, by investigating the photoelectric properties, we found that the MAI-terminated is superior to PbI_2 -terminated. Fourth, the energy barrier for the diffusion of water molecules on the MAI-terminated was calculated. It was found that the energy barrier of one water molecule is only 0.23 eV, and the diffusion energy barrier decreases with the increase of water molecules. Fifth, we calculated the photoelectric properties of one water molecule diffusion. The photoelectric property of the MAI-terminated gradually decreases with the water diffusion. Our study reveals that the MAI-terminated surface exhibits superior properties compared to the PbI_2 -terminated surface, and that the diffusion of water molecules significantly influences the photoelectric properties of MAPbI_3 , which should be considered in experimental designs.

2. Method

In this work, all DFT calculations were performed on the Vienna ab initio simulation package (VASP 5.4.4).^[19] The Perdew-Burke-Ernzerhof (PBE) function with the generalized gradient approximation (GGA) and the projector-augmented wave (PAW) basis were also used in our calculations.^[20] To make the slab model more logical, we built the model with a vacuum layer of 20 Å in the z-direction, which need to adopt the dipole correction to eliminate the influence of the dipole distance in the z-direction. The cutoff energy of the plane wave basis was set equal to 500 eV and the value of number of data points (NEDOS) was set to 1000. The force on each atom was set to be below 0.02 eV/Å and the energy on each atom was set to be below 10^{-5} eV, as two necessary thresholds to stop structure optimization (OPT). A $3\times 3\times 1$ gamma-centered K-point grid was used for sampling during geometric structure optimization (the K-points test data and encut test are shown in Figure S1). This article builds on

previous research by incorporating van der Waals interactions into the calculations, using the DFT–D3 correction method to optimize the structure more accurately.^[21]

Although the number of adsorbed water molecules is the same, the different positions of the water molecules can still lead to a large difference in the energy of the whole system. To eliminate this pitfall and make the results more accurate, five different models were optimized for each adsorption, as show in Figure S2–S6.

We chose the most stable model for the next investigation. To obtain the accurate system energy, the zero-point energy (ZPE) correction was considered.^[22] Since Gibbs free energy takes into account ZPE and entropy correction, which is more accurate than electron energy. Thus, in this work, we use Gibbs free energy instead of electron energy for the most stable model. The main parameters of AIMD simulation in this article are as follows^[23]: using a Nosé thermostat at a temperature of 300 K, adopting a canonical ensemble (NVT), keeping the lattice constant of the system unchanged, with a time step of 1 femtosecond (fs), simulating a total of 10000 steps, and a total simulation time of 10 picoseconds (ps). The equation of adsorption energy, Gibbs free energy Gibbs adsorption energy and MSD are showing Supporting Information (Equations (1)–(5)).

When calculating the optical properties, the spectral properties of materials were described by dielectric functions. A $6\times 6\times 1$ gamma -centered K-point grid was selected for calculation. The equation of photoelectric properties are show in Supporting Information (Equations (6)).

To obtain an accurate transition state, both climbing-image nudged elastic band (CL-NEB)^[24] and improved dimer method (IDM)^[25] were used. More specifically, the CL-NEB method was applied to roughly locate the structure in the transition state with a force convergence of 0.3 eV/Å and the energy on each atom was set to be below 10^{-5} eV with a K-point of $1\times 1\times 1$. The IDM method was then applied to accurately locate the structure in the transition state with a force convergence of 0.05 eV/Å, and the energy on each atom was set to be below 10^{-5} eV with a K-point which same settings as OPT. The equation of reaction energy barrier (G_b) is show in Supporting Information (Equations (7)–(8)).

3. Result and Discussion

3.1. Models

MAPbI_3 has two typical crystal structures: a tetragonal phase (300 K) and an orthorhombic phase (< 162 K).^[26] Here, to make the model more realistic in this work, we chose the tetragonal phase model. The lattice constants of the model used in this work are $a=8.53$ Å, $b=9.27$ Å, $c=12.91$ Å, which highly consistent with previous studies.^[27] Previous research has shown that one of the most typical surface for MAPbI_3 is the (001) surface.^[28] For this reason, we built the model displayed in Figure 1. Each lead atom is surrounded by six iodine atoms, forming a classical octahedral structure. To save resources, we

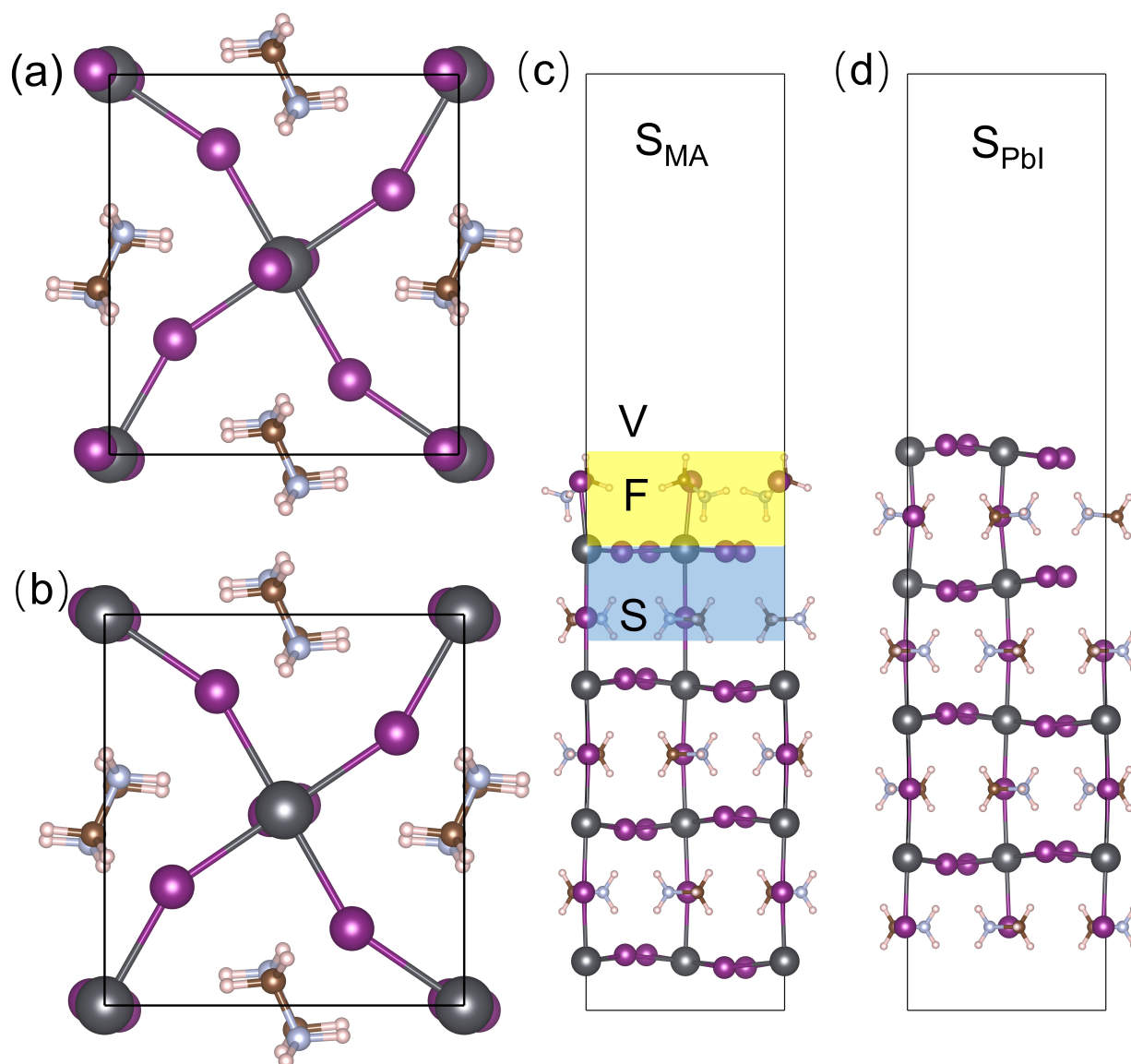


Figure 1. (a) The top view of MAI-terminated (b) The top view of PbI₂-terminated (c) The front view of MAI-terminated (d) The front view of PbI₂-terminated.

only release the first three layers and fix the bottom five layers. To better describe this work, we defined S_{MA} and S_{PbI_2} , where S_{MA} and S_{PbI_2} stand for the MAI-terminated surfaces and PbI₂-terminated surfaces, respectively. In addition, to better discuss the diffusion of water molecules and S_{MA} , we set up the following regions: vacuum regions (V), first regions (F), and second regions (S), as show in Figure 1c.

The most stable model and its adsorption energy of water molecules are shown in Figure 2. The water molecules tend to combine through hydrogen bonds, which means that the presence of hydrogen bonds between water molecules makes the model more stable. As shown in Figure 2a, the Gibbs adsorption energy of one water molecule adsorbed on S_{MA} is 0.18 eV and increases with the number of adsorbed water molecules. As shown in Figure 2b, the Gibbs adsorption energy of one water molecule on the S_{PbI_2} reaches 0.46 eV. As the number of water molecules gradually increases to 9, the Gibbs

adsorption energy on the S_{PbI_2} also gradually increases to 0.55 eV. The Gibbs adsorption energy on the S_{MA} is smaller than that on the S_{PbI_2} , which may be due to the strong oxidation of lead atoms. Lead atoms form strong bonds with oxygen atoms, prompting water molecules to preferentially aggregate on the S_{PbI_2} surface, which may facilitate a reaction between water molecules and MAPbI₃.

3.2. Stability

To gain a deeper explore of the role of water on MAPbI₃, AIMD were performed as shown in Figures 3a and b. We only select the data between 1000 steps and 10000 steps due to the system needs to be balanced. Although the energy fluctuations in these simulations are minimal, the bonds in S_{MA} and $S_{MA}-9H_2O$ remain intact, whereas the bonds in S_{PbI_2} and $S_{PbI_2}-9H_2O$ are

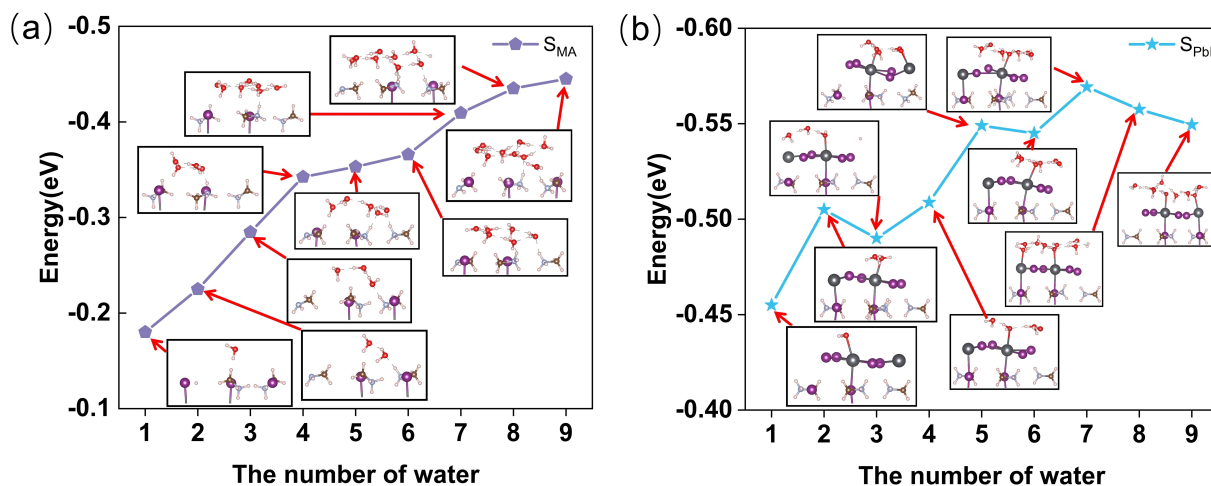


Figure 2. (a) The adsorption energy of MAI-terminated (b) The adsorption energy of PbI_2 -terminated.

disrupted. This means that S_{MA} is more stable than S_{Pbl} , which is the same conclusion as Zhao.^[29]

To further understand the changes between the initial and final states of these four models, XRD analysis was performed. We believe that the changes in the diffraction peaks indicate material decomposition, which in turn suggests a reduction in stability. As shown in Figure 3c and e, the positions and peaks of the diffraction peaks of the initial and final states of the S_{MA} and $S_{\text{MA}}-9\text{H}_2\text{O}$ do not change much after 10000 simulation steps. As shown in Figure 3d, a large number of diffraction peaks appear near 10° after going through 10,000 steps of simulation. These diffraction peaks also appear in the final state in Figure 3f. However, the diffraction peaks in the S_{Pbl} do not change much, while the diffraction peaks in the $S_{\text{Pbl}}-9\text{H}_2\text{O}$ decrease substantially. The variation of diffraction peaks further confirms that S_{MA} is more stable than S_{Pbl} in humid environment, which is consistent with Lu.^[16]

To explore the stability in more depth, MSD were calculated. The diffusivity of lead ions on the S_{MA} is 1.29×10^{-6} and that of iodide ions is 3.21×10^{-6} , as shown in Figure 4a and b. In contrast, the diffusivity of lead ions in the S_{Pbl} reaches 1.21×10^{-4} and that of iodide ions is 1.52×10^{-4} . The diffusivity of lead ions and iodide ions on the S_{Pbl} is two orders of magnitude higher than that on the S_{MA} , further revealing that the S_{MA} is more stable. After adsorption of 9 water molecules, the ion diffusivity of S_{MA} and S_{Pbl} slightly increased but were in the same order of magnitude, as shown in Figure 4c and d.

3.3. Photoelectric Properties

To explore the electron distribution of MAPbI_3 system, the PDOS were calculated as shown in Figure S8. The PDOS in Figure S8 is symmetrical, suggesting that spin polarization has little effect on the system. The energy contribution of the band is predominantly derived from the electron orbitals of Pb and I, with the valence band primarily composed of the p orbitals of I,

and the conduction band mainly consisting of the p orbitals of Pb. This is consistent with earlier research.^[30]

The bandgap has an impact on solar cell usage in addition to being a key factor in optical performance.^[31] In this work, we use the PBE function to determine the bandgap.^[32] As shown in Figure 5a and b, MAPbI_3 is a great photovoltaic material due to its bandgap is a direct bandgap, which allowing electrons in the valence band to jump directly into the conduction band without the need for phonons.^[33] Figure 5e illustrates the absorption coefficient. In reality, MAPbI_3 primarily absorb visible light with wavelengths between 380 nm and 760 nm.^[34] To better describe the absorption coefficient, we defined the E_p (phonon energy), i.e., calculated the area enclosed by the optical absorption coefficient and the x-axis in the visible range, as shown in Table 1. The optical absorption coefficients of S_{MA} and S_{Pbl} are basically the same, and the absorption coefficients decrease with increasing wavelength in the visible range. However, after the adsorption of 9 water molecules, the absorption coefficient of the $S_{\text{MA}}-9\text{H}_2\text{O}$ are basically the same, while the absorption coefficient of the $S_{\text{Pbl}}-9\text{H}_2\text{O}$ decreases. The joint density of states (JDOS) determines the total number of electron transition under the light and can be used as a measure of how much current a material can generate. To quantify the JDOS, we calculated the slope of the K_{JDOS} (slope of the JDOS curve), as shown in Table 1. It can be clearly found that the JDOS of S_{MA} is smaller than that of S_{Pbl} , which means that the current generated by S_{MA} under light is smaller than that generated by S_{Pbl} , as shown in Figure 6. After adsorption of 9 water molecules, the JDOS of S_{MA} is basically unchanged. However, the JDOS of S_{Pbl} decrease substantially, revealing that moisture basically have no change in the photoelectric properties of S_{MA} ,

Table 1. The photoelectric properties of MAPbI_3 .				
	S_{MA}	$S_{\text{MA}}-9\text{H}_2\text{O}$	S_{Pbl}	$S_{\text{Pbl}}-9\text{H}_2\text{O}$
E_p	45327384	45757858	44733907	39544228
K_{JDOS}	54.26	54.26	63.84	26.33

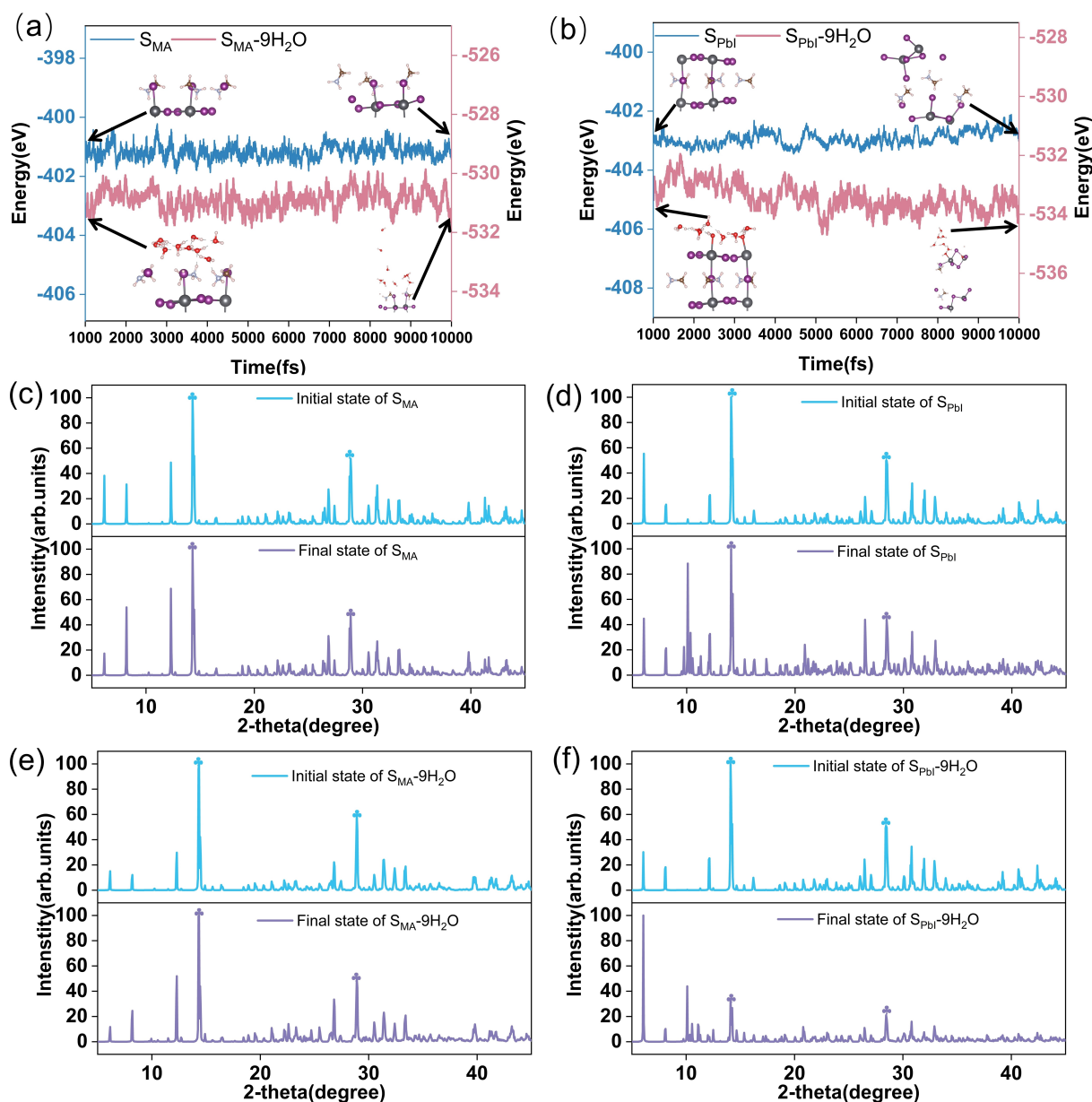


Figure 3. (a) The energy of S_{MA} and S_{MA-9H_2O} (b) The energy of S_{PbI_2} and $S_{PbI_2-9H_2O}$ (c) The XRD of S_{MA} (d) The XRD of S_{PbI_2} (e) The XRD of S_{MA-9H_2O} (f) The XRD of $S_{PbI_2-9H_2O}$.

however, as for the S_{PbI_2} , moisture substantially aligns the photoelectric properties of S_{PbI_2} .

To comprehensively evaluate the overall performance of different surfaces with and without water environments, we plotted the radar map of $MAPbI_3$, as shown in Figure 6. To make the data more expressive, we took the reciprocal of the absolute value of the Gibbs adsorption energy. Through integrated comparison, MAI-terminated surface is superior to PbI_2 -terminated surface, which is consistent with Ambrosio.^[35] In addition, the dielectric constant is also a critical photoelectric property.^[36] Here, the dielectric constants were calculated as shown in Table 2. Unlike the dielectric constants in the xx and yy directions, the dielectric constant in the zz direction is very low, which may be caused by the choice of the slab model. The

Table 2. The dielectric constants of two surfaces.

	ϵ_{std}^{xx}	ϵ_{std}^{yy}	ϵ_{std}^{zz}
S_{MA}	7.24	7.07	1.94
S_{PbI_2}	6.84	6.63	1.90

two exposed surfaces appear one after another due to the difference in annealing time during the fabrication of $MAPbI_3$ films.^[16] Here, we propose a method to detect whether the exposed surface is MAI-terminated surface or PbI_2 -terminated surface by going to the dielectric constant of the film, with the larger dielectric constant being the MAI-terminated surface and

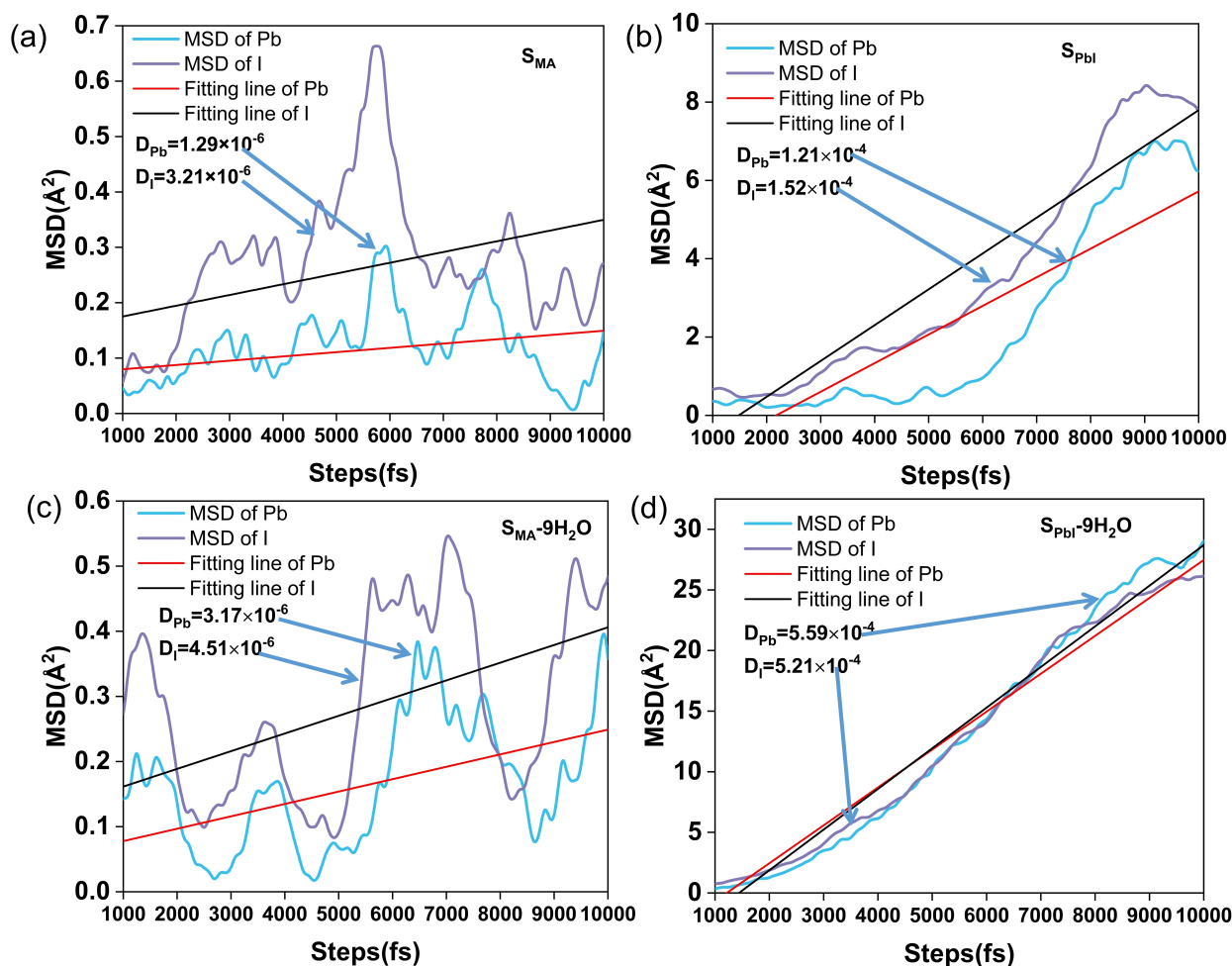


Figure 4. (a) The MSD of S_{MA} (b) The MSD of S_{PbI} (c) The MSD of S_{MA-9H_2O} (d) The MSD of S_{PbI-9H_2O} .

the smaller dielectric constant being the PbI_2 -terminated surface.

3.4. Water Diffusion

During the operation of perovskite solar cells, water molecules are not only adsorbed onto the surface of $MAPbI_3$ but also diffuse into its interior, significantly influencing the properties of $MAPbI_3$.^[37] We focus on water diffusion on S_{MA} through the description above. Three diffusion paths were calculated, as shown in Figure 7. IS represents the initial state, IM1 is the intermediate state, FS is the final state, and TS1 and TS2 are the transition states. It found that the diffusion energy barrier of water molecules is only 0.23 eV, which means that the diffusion of water molecules is extremely easy to occur.^[38] To make matters worse, $MAPbI_3$ is a mass composed of Pb and I frames.^[39] Although there is the presence of organic ion MA^+ , the internal void is large, which provides a favorable environment for water diffusion. It is worth noting that the structure of $MAPbI_3$ also changes greatly as water diffuses from the V region into the F region, which is the same as the research.^[38] The diffusion energy barrier of water molecules from the F region to

the S region is 0.35 eV, revealing that the diffusion on the surface is easier than internal diffusion. Since there are two cases of adsorption of water molecules on the surface, one is two separate water molecules, and the other is the formation of dimer through hydrogen bonding between two water molecules. The diffusion energy barrier of these two cases is calculated respectively, as shown in Figure 7. When two independent water molecules were adsorbed on the surface, the diffusion energy barrier of water molecules from V region to F region decreases from 0.23 eV to 0.10 eV, and the diffusion energy barrier from F region to S region decreases from 0.35 eV to 0.31 eV. The diffusion energy barriers of two water molecules forming dimers are 0.09 eV and 0.29 eV respectively. Although the distribution of water molecules in these two cases is different, the diffusion energy barriers of the two are particularly similar, indicating that the hydrogen bond between water molecules has little influence on the diffusion energy barrier. Water molecules can diffuse into $MAPbI_3$ more readily as the number of water molecules increases, and the influence on diffusion in the V region to F region is greater than that in the F region to S region.

Figure 8 demonstrates the photoelectric effect of one water molecules diffusion. As shown in Figure 8a, the bandgap of the

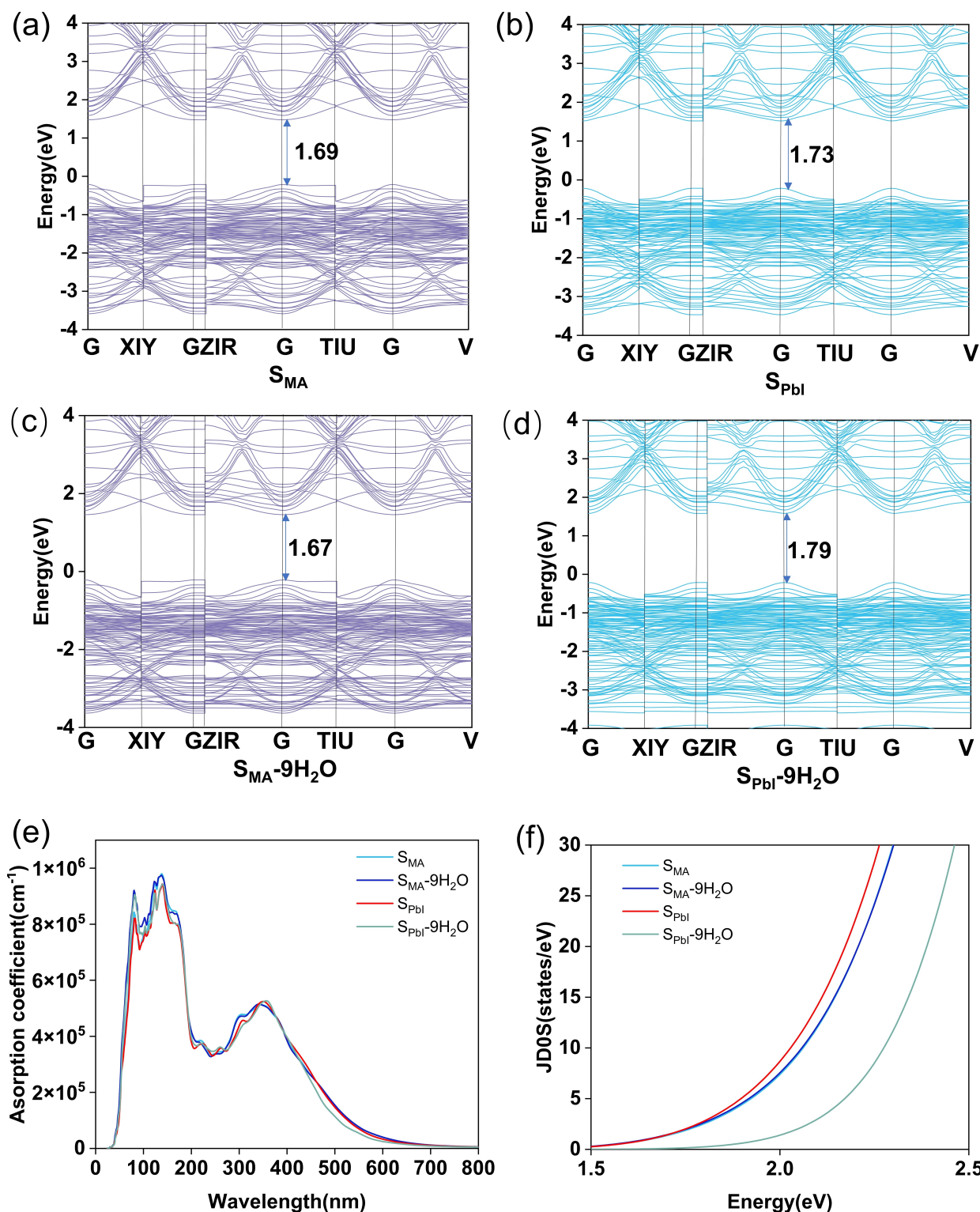
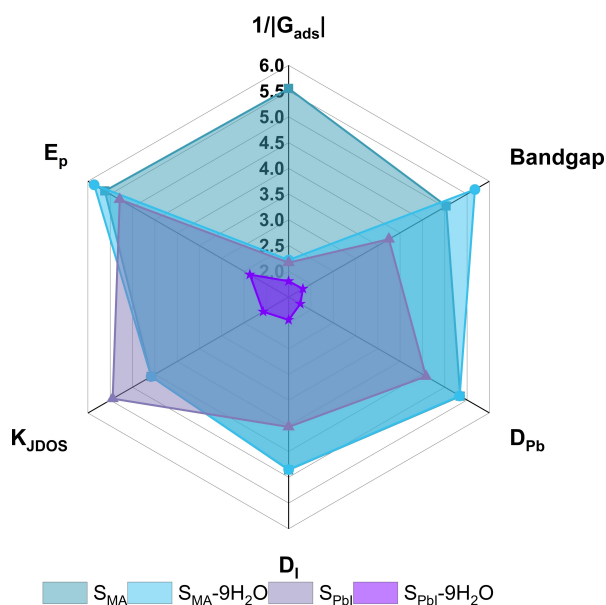


Figure 5. (a) The bandgap of S_{MA} (b) The bandgap of S_{PbI} (c) The bandgap of S_{MA-9H_2O} (d) The bandgap of S_{PbI-9H_2O} (e) The absorption coefficient of S_{MA} , S_{PbI} , S_{MA-9H_2O} and S_{PbI-9H_2O} (f) The JDOS of S_{MA} , S_{PbI} , S_{MA-9H_2O} and S_{PbI-9H_2O} .

S_{MA} decreases from 1.69 eV to 1.67 eV after adsorption of a water molecule. Then, the bandgap increases from 1.67 eV to 1.71 eV as the water molecule diffuses from the O region to the F region (Figure 8b). The bandgap increases from 1.71 eV to 1.72 eV when diffusing from the F region to the S region

(Figure 8c). The bandgap reveals that the diffusion of the water molecule causes a photoelectric properties effect decrease, especially in the diffusion from the O region to the F region. Figure 8d illustrates the absorption coefficient of the diffusion process. It can be found that the absorption coefficients of the

Figure 6. The radio map of MAPbI₃.

3 models are basically constant during the diffusion process. However, the JDOS continues to decrease as the diffusion proceeds downward during the diffusion process, which means that the diffusion of one water molecules reduces the total number of electron transition under the light, as shown in Figure 8e.

4. Conclusions

The stability and photoelectric properties of the different exposed surfaces of MAPbI₃ has been verified by DFT calculated. The Gibbs adsorption energy of one water molecules adsorbed on the PbI₂-terminated surface (0.46 eV) is slightly higher than that of water molecules adsorbed on the MAI-terminated surface (0.18 eV), implying that water molecules are more likely to aggregate on the PbI₂-terminated. The result of AIMD, XRD and MSD reveal that the MAI-terminated is more stable than PbI₂-terminated in dry environments. As 9 water molecules are adsorbed, the MAI-terminated is also more stable than the PbI₂-terminated. The absorption coefficient and JDOS of MAPbI₃ are basically affected by the water molecules, while the absorption coefficient and JDOS of PbI₂-terminated decrease with 9 water

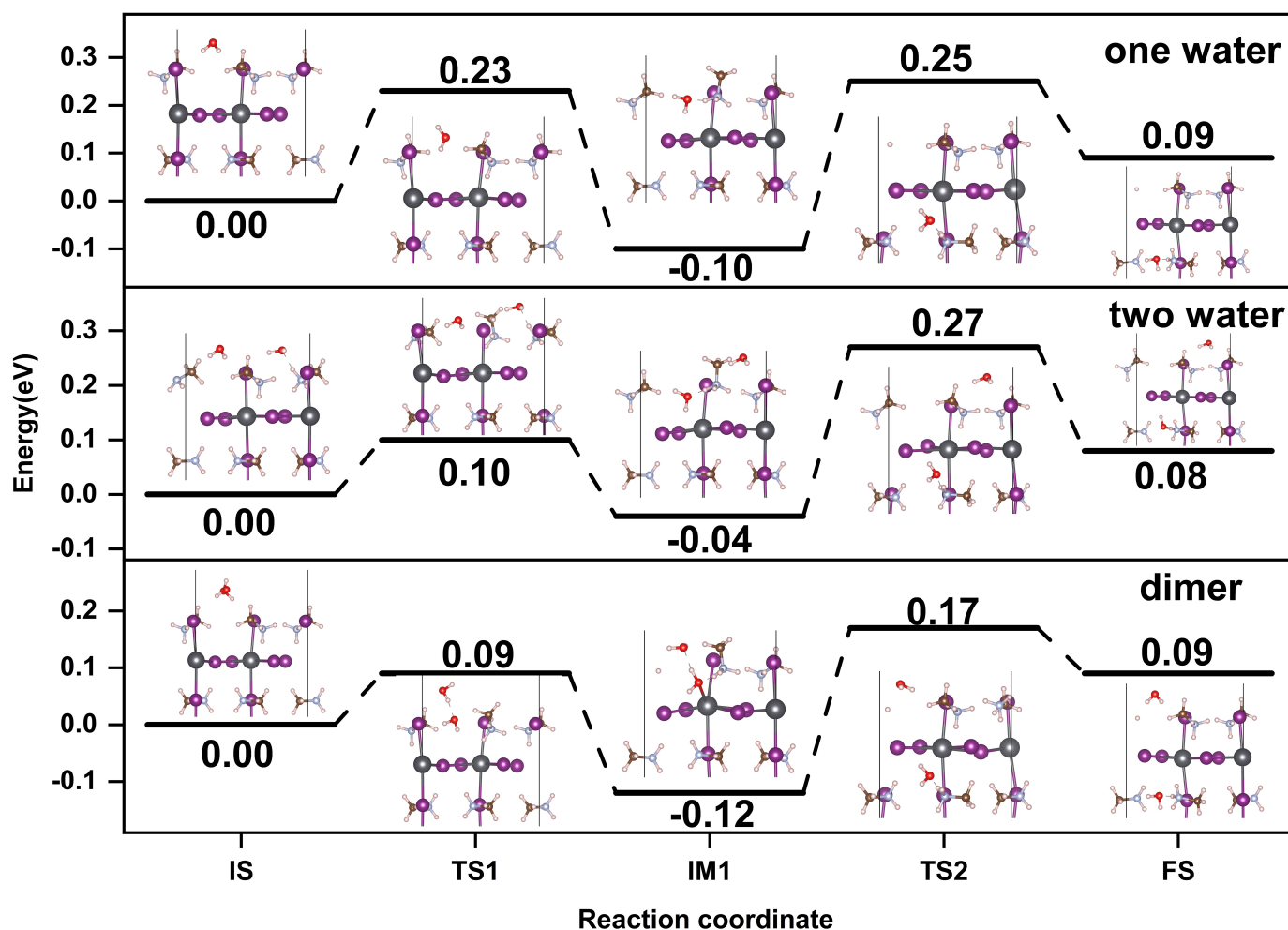


Figure 7. Diffusion of water molecules under different conditions.

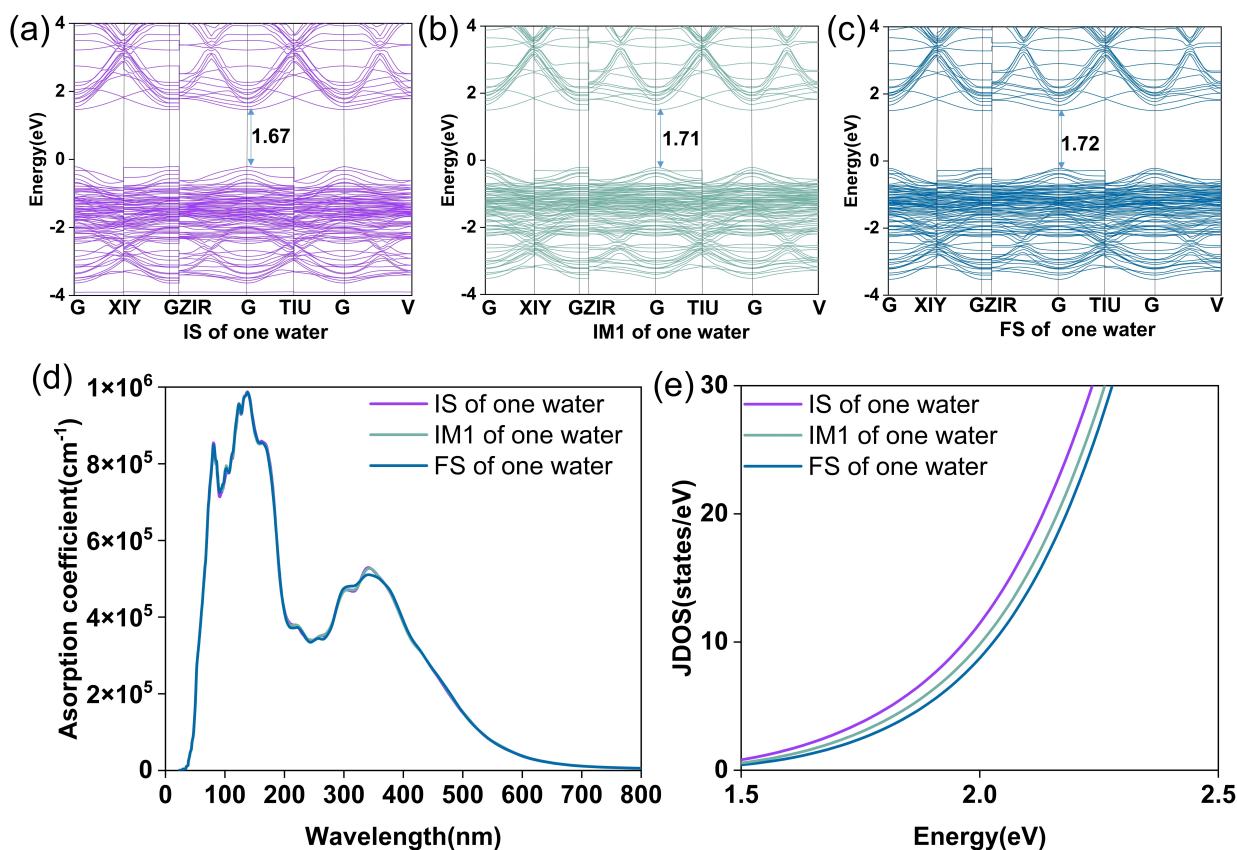


Figure 8. (a) The bandgap of IS (b) The bandgap of IM1 (c) The bandgap of FS (d) The absorption coefficient of one water diffusion systems (e) The JDOS of diffusion one water diffusion systems.

molecules are adsorbed. The energy barrier of one water diffusion is 0.23 eV, which reveals that water molecules can spread easily into the interior of the MAPbI₃. As the number of water molecules increases to two, diffusion gets even easier. More importantly, the diffusion of water leads to a decrease in the photoelectric properties of MAPbI₃. We fervently urge paying close attention to the MAPbI₃ exposed surface during the thin film production process and changing synthesis settings to create thin films with a dominant MAI-terminated surface, which should significantly enhance the performance of MAPbI₃ in the application.

Acknowledgements

H. Li acknowledges the Center for Computational Materials Science, Institute for Materials Research, Tohoku University for the use of MASAMUNE-IMR (202312- SCKXX-0203) and the Institute for Solid State Physics (ISSP) at the University of Tokyo for the use of their supercomputers.

Conflict of Interests

There are no conflicts to declare.

Data Availability Statement

The data that support the findings of this study are available from the corresponding author upon reasonable request.

Keywords: MAPbI₃ · MAI-terminated · Pbl₂-terminated · Humid · Stably · Photoelectric properties · Diffusion

- [1] A. Kojima, K. Teshima, Y. Shirai, T. Miyasaka, *J. Am. Chem. Soc.* **2009**, *131*, 6050–6051.
- [2] a) M. Azam, S. Yue, R. Xu, K. Liu, K. Ren, Y. Sun, J. Liu, Z. Wang, S. Qu, Y. Lei, Z. Wang, *J. Mater. Chem. A* **2018**, *6*, 13725–13734; b) C. C. Stoumpos, C. D. Malliakas, M. G. Kanatzidis, *Inorg. Chem.* **2013**, *52*, 9019–9038; c) S. D. Stranks, G. E. Eperon, G. Grancini, C. Menelaou, M. J. P. Alcocer, T. Leijtens, L. M. Herz, A. Petrozza, H. J. Snaith, *Science* **2013**, *342*, 341–344; d) W. J. Yin, T. Shi, Y. Yan, *Adv. Mater.* **2014**, *26*, 4653–4658; e) D. B. Mitzi, *Prog. Inorg. Chem.* **1999**, 1–121; f) Y. Chen, X. Ding, L. Yang, Y. Wang, J. I. Gurti, M. Wang, W. Li, X. Wang, W. Yang, *PCCP* **2022**, *24*, 14375–14389.
- [3] Y. Hou, E. Aydin, M. De Bastiani, C. Xiao, F. H. Isikgor, D.-J. Xue, B. Chen, H. Chen, B. Bahrami, A. H. Chowdhury, A. Johnston, S.-W. Baek, Z. Huang, M. Wei, Y. Dong, J. Troughton, R. Jalmoood, A. J. Mirabelli, T. G. Allen, E. Van Kerschaver, M. I. Saidaminov, D. Baran, Q. Qiao, K. Zhu, S. De Wolf, E. H. Sargent, *Science* **2020**, *367*, 1135–1140.
- [4] Z. Gao, Y. Bai, M. Wang, G. Mao, X. Liu, P. Gao, W. Yang, X. Ding, J. Yao, *J. Phys. Chem. C* **2022**, *126*, 13409–13415.
- [5] a) D. C. Miller, H. I. Khonkar, R. Herrero, I. Antón, D. K. Johnson, T. Hornung, T. Schmid-Schirling, T. B. Vinzant, S. Deutch, B. To, G. Sala, S. R. Kurtz, *Solar Energy Mater. Solar Cells* **2017**, *167*, 7–21; b) Y.-S. Kim, C.-H. Ri, Y.-H. Kye, U.-G. Jong, X. Wang, Y. Zhang, X. Niu, C.-J. Yu, *J. Phys. Chem. C* **2022**, *126*, 3671–3680.

- [6] a) M. Li, H. Li, J. Fu, T. Liang, W. Ma, *J. Phys. Chem. C* **2020**, *124*, 27251–27266; b) Y. Yang, T. Chen, D. Pan, J. Gao, C. Zhu, F. Lin, C. Zhou, Q. Tai, S. Xiao, Y. Yuan, Q. Dai, Y. Han, H. Xie, X. Guo, *Nano Energy* **2020**, *67*, 104246.
- [7] a) Y. Chen, X.-L. Ding, H.-B. He, Y.-Y. Wang, S.-P. Xu, M.-M. Wang, W. Li, *J. Mater. Chem. A* **2023**; b) X. Liu, Y. Bai, S. Chen, C. Wu, I. D. Gates, T. Huang, W. Li, W. Yang, Z. Gao, J. Yao, X. Ding, *J. Mol. Model.* **2022**, *28* (80), 1–11.
- [8] J. Zhao, B. Cai, Z. Luo, Y. Dong, Y. Zhang, H. Xu, B. Hong, Y. Yang, L. Li, W. Zhang, C. Gao, *Sci. Rep.* **2016**, *6*, 21976.
- [9] M. Liu, M. B. Johnston, H. J. Snaith, *Nature* **2013**, *501*, 395–398.
- [10] J. You, Y. Yang, Z. Hong, T.-B. Song, L. Meng, Y. Liu, C. Jiang, H. Zhou, W.-H. Chang, G. Li, Y. Yang, *Appl. Phys. Lett.* **2014**, *105*, 183902.
- [11] M. Kim, H. Kim, J. Sin, M. Kim, G. Kim, J. Kim, W. Kim, B. Kim, K. Lee, H. M. Oh, J. Sung, H.-K. Choi, M. S. Jeong, J. Hong, J. Yang, *Chem. Eng. J.* **2024**, *497*, 154821.
- [12] Z. Zhu, V. G. Hadjiev, Y. Rong, R. Guo, B. Cao, Z. Tang, F. Qin, Y. Li, Y. Wang, F. Hao, S. Venkatesan, W. Li, S. Baldelli, A. M. Guloy, H. Fang, Y. Hu, Y. Yao, Z. Wang, J. Bao, *Chem. Mater.* **2016**, *28*, 7385–7393.
- [13] G. E. Eperon, S. N. Habisreutinger, T. Leijtens, B. J. Bruijns, J. J. van Franeker, D. W. deQuilettes, S. Pathak, R. J. Sutton, G. Grancini, D. S. Ginger, R. A. J. Janssen, A. Petrozza, H. J. Snaith, *ACS Nano* **2015**, *9*, 9380–9393.
- [14] Y. Dong, K. Li, W. Luo, C. Zhu, H. Guan, H. Wang, L. Wang, K. Deng, H. Zhou, H. Xie, Y. Bai, Y. Li, Q. Chen, *Angew. Chem. Int. Ed.* **2020**, *59*, 12931–12937.
- [15] E. Mosconi, J. M. Azpiroz, F. De Angelis, *Chem. Mater.* **2015**, *27*, 4885–4892.
- [16] Y. Lu, Z. Si, H. Liu, Y. Ge, J. Hu, Z. Zhang, X. Mu, K. Selvakumar, M. Sui, *Chem. A Europ. J.* **2021**, *27*, 3729–3736.
- [17] S. Nachimuthu, M. Q. Cai, Y. C. Wang, et al., *Mater. Today Adv.* **2023**, *18*, 100370.
- [18] Y. Ouyang, L. Shi, Q. Li, J. Wang, *Small Methods* **2019**, *3*, 1900154.
- [19] a) G. Kresse, J. Furthmüller, *Phys. Rev. B* **1996**, *54*, 11169–11186. b) G. Kresse, J. Furthmüller, *Comput. Mater. Sci.* **1996**, *6*, 15–50.
- [20] J. P. Perdew, K. Burke, M. Ernzerhof, *Phys. Rev. Lett.* **1996**, *77*, 3865–3868.
- [21] S. Grimme, J. Antony, S. Ehrlich, H. Krieg, *J. Chem. Phys.* **2010**, *132*, 154104.
- [22] a) J. Zhao, Z. Chen, *J. Am. Chem. Soc.* **2017**, *139*, 12480–12487. b) C. Ling, L. Shi, Y. Ouyang, X. C. Zeng, J. Wang, *Nano Lett.* **2017**, *17*, 5133–5139. c) K. Reuter, M. Scheffler, *Phys. Rev. B* **2001**, *65*
- [23] Z. Gao, M. Wang, H. Zhang, S. Chen, C. Wu, I. D. Gates, W. Yang, X. Ding, J. Yao, *Solar Energy Mater. Solar Cells* **2021**, *233*.
- [24] a) G. Henkelman, B. P. Uberuaga, H. Jónsson, *J. Chem. Phys.* **2000**, *113*, 9901–9904. b) G. Henkelman, H. Jónsson, *J. Chem. Phys.* **2000**, *113*, 9978–9985.
- [25] A. Heyden, A. T. Bell, F. J. Keil, *J. Chem. Phys.* **2005**, *123*, 224101.
- [26] K. Yukihiro, H. Mashiyama, K. Hasebe, *J. Phys. Soc. Japan* **2002**, *71*, 1694–1697.
- [27] T. Baikie, Y. Fang, J. M. Kadro, M. Schreyer, F. Wei, S. G. Mhaisalkar, M. Graetzel, T. J. White, *J. Mater. Chem. A* **2013**, *1*, 5628–5641.
- [28] H. Zhang, H. Huang, K. Haule, D. Vanderbilt, *Phys. Rev. B* **2014**, *90*.
- [29] Y. Zhao, L. Cheng, B. Xu, L. Meng, *Comput. Mater. Sci.* **2023**, *219*, 112028.
- [30] J. Haruyama, K. Sodeyama, L. Han, Y. Tateyama, *J. Phys. Chem. Lett.* **2014**, *5*, 2903–2909.
- [31] Z. Xiao, Y. Zhou, H. Hosono, T. Kamiya, N. P. Padture, *Chem. A Europ. J.* **2018**, *24*, 2305–2316.
- [32] Z. Gao, G. Mao, S. Chen, Y. Bai, P. Gao, C. Wu, I. D. Gates, W. Yang, X. Ding, J. Yao, *PCCP* **2022**, *24*, 3460–3469.
- [33] P. Basumatary, P. Agarwal, *J. Mater. Sci. Mater. Electron.* **2020**, *31*, 10047–10054.
- [34] H. Zhong, Z. Liu, P. Tang, X. Liu, X. Zhan, P. Pan, C. Tang, *Sol. Energy* **2020**, *208*, 445–450.
- [35] F. Ambrosio, D. Meggiolaro, E. Mosconi, F. De Angelis, *J. Mater. Chem. A* **2020**, *8*, 6882–6892.
- [36] C. C. Homes, T. Vogt, S. M. Shapiro, S. Wakimoto, A. P. Ramirez, *Science* **2001**, *293*, 673–676.
- [37] a) N. Z. Koocher, D. Saldana-Greco, F. Wang, S. Liu, A. M. Rappe, *J. Phys. Chem. Lett.* **2015**, *6*, 4371–4378. b) F. Tian, W. Feng, B. Xing, X. He, W. A. Saidi, L. Zhang, *Adv. Energy Sustain. Res.* **2021**, *2*, 2100087.
- [38] C.-J. Tong, W. Geng, Z.-K. Tang, C.-Y. Yam, X.-L. Fan, J. Liu, W.-M. Lau, L.-M. Liu, *J. Phys. Chem. Lett.* **2015**, *6*, 3289–3295.
- [39] L. Zhang, P. H. L. Sit, *J. Phys. Chem. C* **2015**, *119*, 22370–22378.

Manuscript received: September 17, 2024

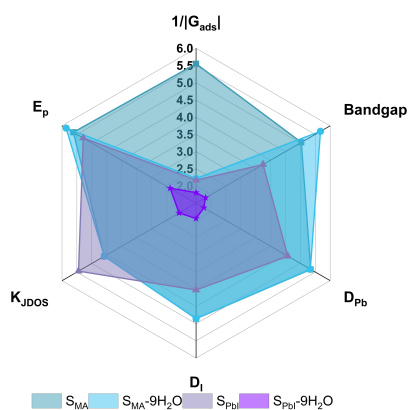
Revised manuscript received: October 18, 2024

Accepted manuscript online: November 5, 2024

Version of record online: ■■, ■■

RESEARCH ARTICLE

The exposed surface characteristics of $\text{CH}_3\text{NH}_3\text{PbI}_3$ (MAPbI₃) are crucial for its stability and photoelectric performance under humid conditions. This study shows that MAI-terminated surfaces outperform PbI_2 -terminated surfaces in both aspects, based on density functional theory calculations. Optimizing synthesis parameters to produce MAI-terminated films is key to enhancing MAPbI₃ photovoltaic applications.



B. Zhang, R. Shi, H. Ma, K. Ma, Z. Gao, H. Li*

1 – 11

Revisiting the Exposed Surface Characteristics on the Stability and Photoelectric Properties of MAPbI₃

